Aalborg Universitet

Frozen Leg Operation of a Three-Phase Dual Active Bridge Converter

Haghbin, Saeid; Blaabjerg, Frede; Bahman, Amir Sajjad

Frozen Leg Operation of a Three-Phase Dual Active Bridge Converter

Saeid Haghbin, *Senior Member, IEEE,* Frede Blaabjerg, *Fellow, IEEE,* and Amir Sajjad Bahman, *Member, IEEE*

Abstract—Three-phase dual active bridge (DAB) topology is a potential alternative for high-power applications when a compact and efficient converter with a bidirectional power transfer capability is desired. In a constructed prototype high-power SiC modules with dedicated drivers are utilized to achieve high-efficiency and compact size. Each module has two interconnected switches with anti-parallel diodes resembling a converter leg. It is observed that the driver halts the module operation as a result of protective actions such as over-current, gate under-voltage, or gate over-voltage. In this frozen leg mode, the module operates as a leg with two diodes until an external hardware signal resets the driver. The converter continues operation but with a reduced performance. Analysis, simulation and verification of a three-phase DAB converter under a frozen leg operation are considered in this paper. The converter with a frozen leg has two different behaviours at light loads and heavy loads. Consequently, two different analysis methods are developed to solve converter operation in different load conditions. Results show that the power transfer capability is reduced, but this fault mode is non-destructive.

I. INTRODUCTION

The three-phase DAB topology is one of the circuit candidates for the DC/DC conversion stage to achieve a high-power density while keeping the efficiency high [1]–[6]. One major drawback of the DAB configuration in the three-phase version is the high number of switches and drivers compared to its single-phase variant. Hence, the risk of failure in a switch including the drivers and auxiliary circuits are higher than in a topology with fewer components such as a single-phase DAB converter [7], [8].

In a constructed prototype based on a three-phase DAB converter for the DC/DC stage, SiC-based $300\ A/1200\ V$ modules and dedicated drivers from CREE are used. The power modules are CAS300M12BM2 and the drivers are PT62SCMD12. This SiC power module has two switches in series to be used as a leg in the converter. Anti-parallel diodes are also included in the module. The gate driver is using an isolating scheme with some protection features. The driver protects the upper and lower switches in the module for the drain over-current and the gate power supply under-voltage and over-voltage.

There are different failure scenarios demanding a comprehensive investigation and analysis [7], [10]–[13] in order to

achieve a more reliable system. It is observed that the driver freezes the module operation as a protection action provided by the driver. In this case, the driver activates the module after a hardware reset; during this fault mode, the anti parallel diodes are still in operation (assuming that they are healthy).

A frozen leg on the secondary side of the DAB converter is considered in this work. Theoretically there is no difference between the primary and secondary of this converter. Hence, this case can be an appropriate representative for one leg halt mode. The same method can be used for similar cases such as two leg or three leg halt modes.

This topic, halt mode operation of a power module because of the driver protection action, is not typically considered in literature. It is expected with a widely usage of high-power modules in different applications like automotive, this work can demonstrate an example of reliability enhancement of a power converter. As an immediate result, fault mode detection and post-fault strategy are the next questions to be addressed. Those issues are not considered in this work in order to limit the scope. However, by analysing the transformer current it is possible to detect this fault mode. As a post fault strategy, it is possible to reduce the converter power level or overdesign the power module for a safe continuous operation under this halt mode.

In a frozen leg mode of operation, the three-phase DAB converter has two different behaviours. At light load the converter face slight unsymmetry in the phases but when the load increases, this unsymmetry increases and the phase with a frozen leg undergoes a huge change in behaviour compared to a normal mode operation. For an accurate analytical analysis in all line and load conditions, the converter with two active three-phase bridges and body diodes shall be analysed in a frozen leg mode. The number of components including diodes makes this task complicated, if it is not impossible. Hence, the idea of this work is to perform analysis of simpler cases. At light loads where slight unsymmetry affects the converter, the deviation from normal mode of operation is considered. By decomposing the transformer current into the normal and deviated from the normal values, the analysis is performed to calculate the fault current. Consequently, the converter power is calculated at light loads [14].

At heavier loads, which is clarified later on, the transformer current of the halted phase undergoes a considerable deviation from the normal operation value. In this case, a direct analysis method is developed to calculate the fault current. Consequently, the power transfer is calculated also. The results show that after a leg halt, the power transfer capability is reduced enabling to continue operation but with a reduced power.
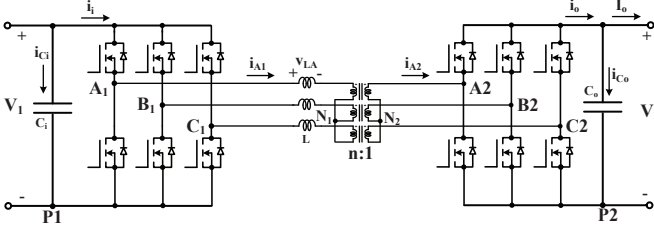
Fig. 1. Equivalent circuit of three-hase DAB converter used in the charger.

The boarder of light load region and heavy load region is analytically calculated using the developed equations for the power transfer under the frozen leg operation mode. The terms light load and heavier load are clarified after presenting the calculated power transfer equations.

After this introduction, the three-phase DAB converter in normal mode with focus on the required background for the frozen leg analysis is presented in section II. The fault current and power calculations at light loads are presented in section III. Section IV is dedicated to the converter analysis under a frozen leg operation at heavier loads. The verifications are presented in the section section, section IV and conclusions are given in the final section.

II. NORMAL OPERATION OF A THREE-PHASE DAB

Fig. 1 shows the power stage of a three-phase DAB circuit topology. The selected polarities for the voltages, currents and different points of the circuit are defined in this figure too. Two active three-phase bridges generate three-phase voltages towards the high-frequency transformer. The transformer inductances and inverter voltages determine the direction and amount of the power flow. There are different methods to control the power transfer in which the phase-shift control is one of the widely used techniques for this bidirectional topology [15] and it is considered in this work. It is assumed that the transformer has a $Y - Y$ configuration where the star points are denoted as N_1 and N_2 for the primary and secondary sides, subsequently.

The energy storage inductors of the circuit, L, can be the transformer leakage inductances or external inductors. To analyze the converter, a lossless model of the transformer is used without considering the magnetizing inductances.

The control of the converter is performed via controlling the gate signals of the bridges in the primary and secondary sides. The phase-shift between the primary and secondary determines the direction and magnitude of the power flow. Fig. 2 shows important waveforms of the converter from the gate command to the transformer waveforms in the primary and secondary sides.

The phase-shift angle φ, the input voltage V_1, the output voltage V_2, the transformer primary to secondary turns ratio n, the switching frequency f and series inductance L determine the power transfer, P_{nom}, as [2]

$$P_{nom} = \frac{n\,V_1 V_2}{\omega L}\varphi\left(\frac{2}{3} - \frac{\varphi}{2\pi}\right) \qquad (1)$$
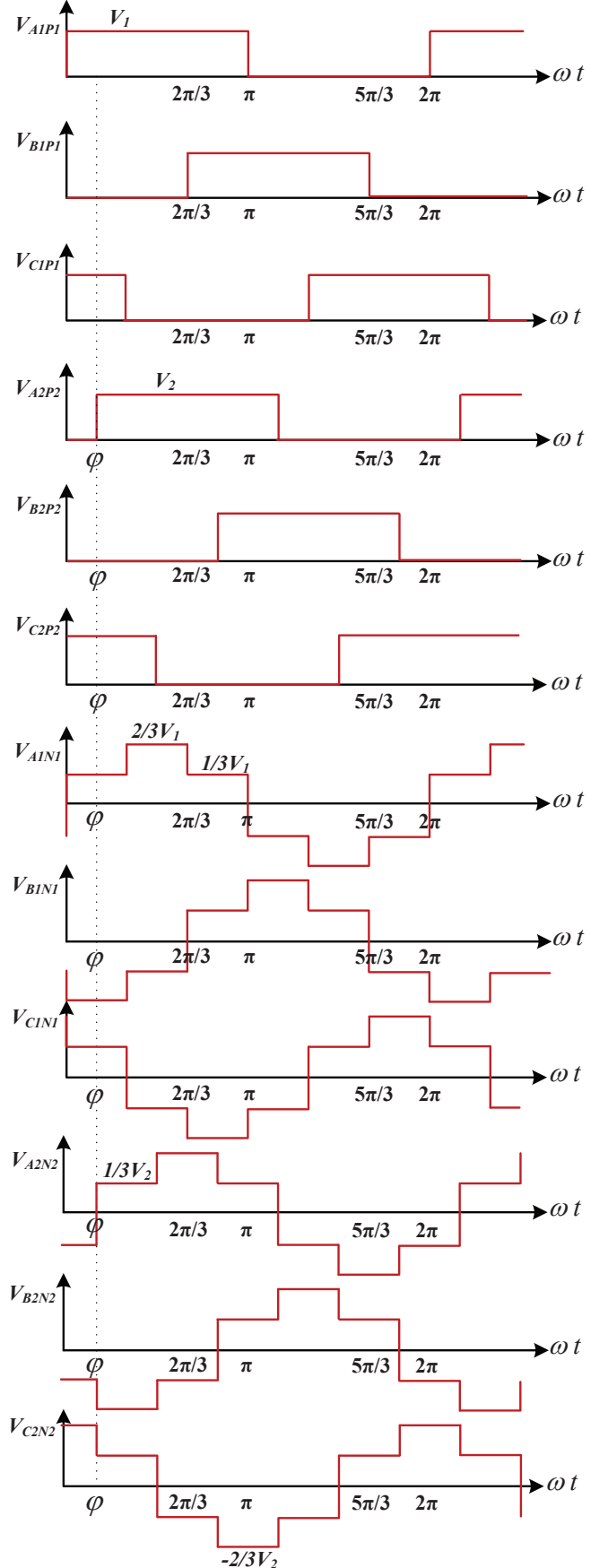

Fig. 2. Ideal waveforms of a three-phase DAB converter shown in Fig. 1.

where $\omega = 2\pi f$ is the angular frequency in rad/s. If the input voltage is equal to the referred output voltage to the primary, i.e. $V_1 = nV_2$, this equation can be written as [2]

$$P_{nom} = \frac{V_1^2}{\omega L}\varphi\ (\frac{2}{3} - \frac{\varphi}{2\pi}).\qquad (2)$$

To analyze the converter operation, firstly the inverter output voltages to the negative dc bus, V_{X1P1}, are calculated where X is either A, B or C. Then the transformer voltages to the star points, V_{X1N1}, are calculated. The transformer voltages and the inverter voltages are used to calculate the inductor voltages. Consequently, one can determine the inductor currents. By multiplication of the inductor currents and transformer voltages, it is possible to determine the power. This is the main procedure to analyze the converter in a normal operation and in a frozen leg mode.

Now assume that V_{C2P2} is slightly changed because of a frozen leg. For example, it is turned on after a delay or turned on earlier than it is planned. This results in a change in the voltage waveforms in the transformer voltages V_{X2N2}. The new waveforms can be calculated very similar to those shown in Fig. 2.

In the case where leg C in the secondary is frozen, V_{C2P2} is deviated from its original shape. Depending on which body diode is conducting, this voltage can be determined. However, to perform an analysis for this case, the same procedure is followed, but with another voltage profile of V_{C2P2}. The inductor voltages and currents are calculated for this case and consequently the power is calculated, which is presented in the next section.

III. ANALYSIS OF A THREE-PHASE DAB CONVERTER UNDER A FROZEN LEG OPERATION AT LIGHT LOADS

The inductor waveforms, three-phase voltages and currents, are shown in Fig. 3 in a normal operating condition [2]. The waveforms are for the condition which $V_1 = nV_2$. This case is easier for analysis and holds through the rest of the paper. The current has a flat waveform in the maximum or minimum condition where the value is I_2. I_1 is the current value in the flat region in the middle. These two values, I_1 and I_2, can describe the current waveform. One part of the inductor voltage is shown by a dashed line and the arrow shows the point of deviation from the original waveform. For frozen leg C, this part of the inductor voltage is affected. This is from the basic waveforms of the converter shown in Fig. 2.

A. Inductor waveforms decomposition to analyse the frozen leg condition at light loads

The width of the dashed-line in the inductor voltage is φ. This is the normal width in a normal operation. It is assumed that some part of this pulse is changed to zero as a result of a frozen leg. Hence, it is assumed that the width of α is changed to zero in the frozen leg condition. The angle α is an arbitrary small angle that can be determined in a certain operating condition of the converter. Simulation and experiments verify this assumption. Consequently, the idea is to solve the circuit when the inductor voltage is deviated from
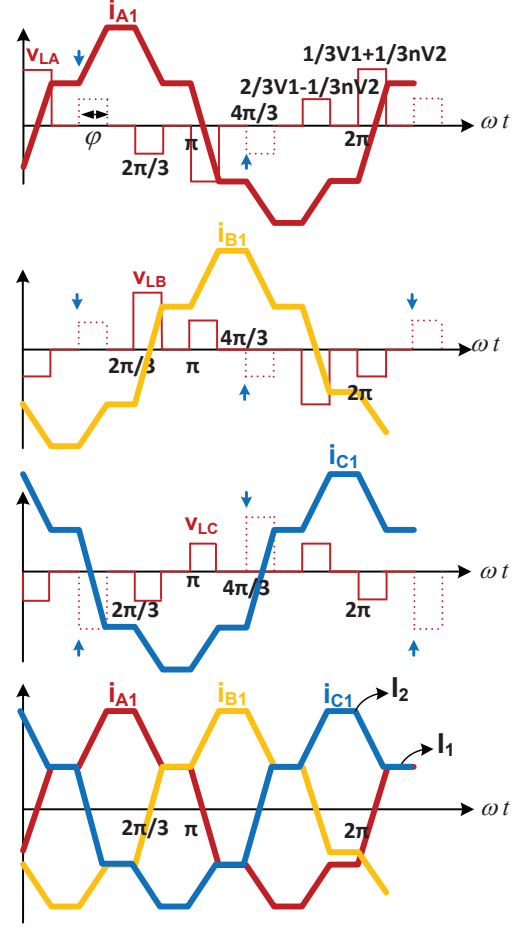

Fig. 3. The inductor waveforms in a three-phase DAB converter.

its normal operation. In this case, the change is that one piece of the inductor voltage in the beginning of the dashed-line area with a width of α is zero.

If α is small, it is possible to use superposition to solve the circuit. It is assumed that the circuit parameters and load conditions are such that the superposition is valid, as it is shown in simulations and experiments. Fig. 4 shows the procedure of decomposing the circuit. The width of α is considered as an addition of the original voltage and a negative voltage. In this way, the current can be calculated as the sum of the normal current and the current resulted by a negative pulse with width of α.

For a normal operation of DAB converter, the analysis is not shown here and one can refer to references [1], [2]. For the inductors with a negative voltage pulse, it is possible to solve the circuit to find the current and later on the resulting power. Fig. 5 shows the voltage and current waveforms as a deviation from normal operation. Phase A and B have similar waveforms while phase C has twice negative value of the current and voltage (sum of three-phase is zero). Note that this waveforms are added to the normal waveforms and can be interpreted as unsymmetrical components.

In steady state condition and considering the inductor flux-balance, the value of the inductor current can be calculated
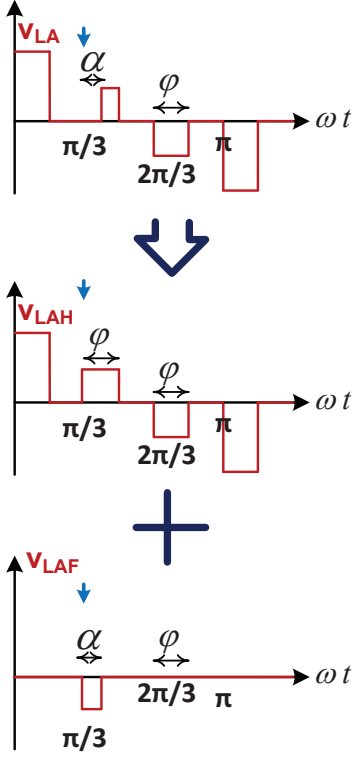
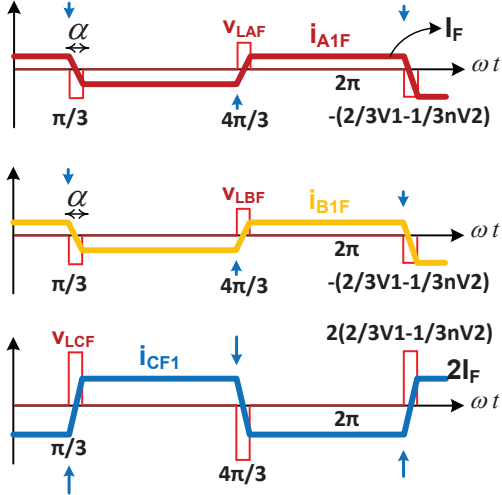Fig. 4. Decomposition of the inductor voltage for the analysis.

Fig. 5. The indutor waveforms for a decompoed negative voltage pulse at light loads.

as

$$I_F = \frac{V_1 \alpha}{6\omega L} \qquad (3)$$

where I_F is the peak current of the inductor and α is the width of voltage pulse in radians.

B. Power transfer calculation for the decomposed fault current at light loads

In this section, detailed calculations of the transferred power after freezing leg C in the secondary side is presented. For the decomposed fault waveform, the inductor currents and
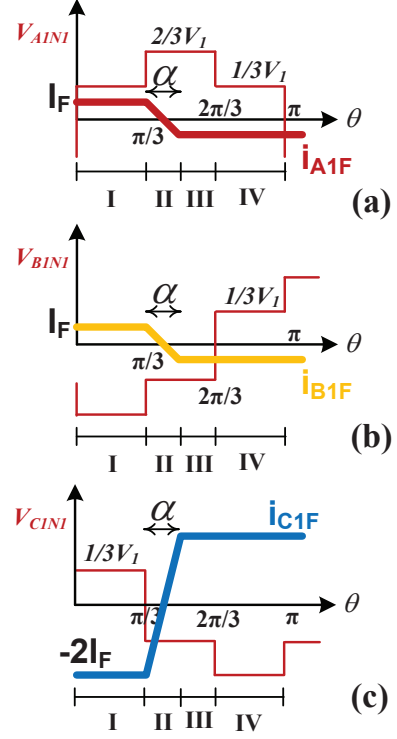
Fig. 6. The transformer waveforms in the primary side after leg C has been frozen at light loads.

transformer voltages are multiplied and averaged over a half cycle, for each phase. The total power is the addition of the power in normal operation mode and the calculated power for the decomposed waveform (negative pulse of the inductor).

The analysis is based on the following assumptions: the input/output voltages are equal to the transformer turns ratio, there is no dead-time, the maximum value of the phase shift is 60°, and the components are ideal. Hence, a slight deviation from the measurement and theoretical values are expected.

Fig. 6a shows the transformer current and voltage for the phase A. A half cycle is divided into four intervals which the power is calculated for each interval and then it is averaged over a half period to calculate the average power as

$$P_{AD} = \frac{1}{\pi} \int_0^\pi V_{A1N1}(\theta) i_{A1}(\theta) d\theta = \qquad (4)$$
$$P_{ADI} + P_{ADII} + P_{ADIII} + P_{ADIV}.$$

For each interval, the power is calculated as

$$P_{ADI} = \frac{1}{\pi}(\frac{1}{3}V_1 I_F \ \pi/3) \qquad (5)$$

$$P_{ADII} = 0 \qquad (6)$$

$$P_{ADIII} = \frac{1}{\pi}(-\frac{2}{3}V_1 I_F \ (\pi/3 - \alpha)) \qquad (7)$$

$$P_{ADIV} = \frac{1}{\pi}(-\frac{1}{3}V_1 I_F \ \pi/3). \qquad (8)$$

The average power value of the phase A can be calculated as

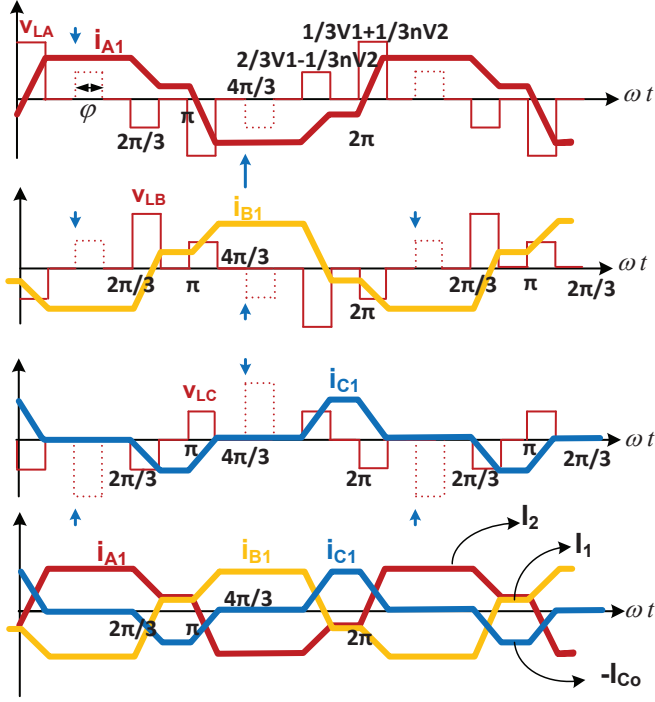$$P_{AD} = -\frac{2}{3}V_1 I_F(\frac{1}{3} - \frac{\alpha}{\pi}). \qquad (9)$$

Fig. 7. Inductor waveforms for analytical analysis after freezing leg C on the secondary side at heavier loads.

Fig. 8. The transformer waveforms in the primary side after leg C has been frozen.

The inductor voltage is calculated as the difference between the primary side bridge voltage and the secondary side bridge voltage referred to the primary side as

$$V_{LX} = V_{X1N1} - n\, V_{X2N2}. \qquad (24)$$

The inductor current is flat because the referred output voltage is equal to the input voltage in this case.

In a three-phase system the sum of the voltages and currents are zero, which can be seen from Fig. 7. The analysis is started from phase C where the current is zero for some intervals. In this case the phase A and B are equal but with 180 degree phase shift. The inductor voltage for phase C includes two pulses, one negative and one positive, which each has a duration of φ. The voltage values are the same as the ones with a nominal condition, which are shown in Fig. 7. The inductor voltage waveform for phase C can uniquely determine the current.

The peak value of the inductor current in phase C is calculated as

$$I_{C_o} = \frac{V_1 \varphi}{3\omega L} \qquad (25)$$

where I_{C_o} is the peak value of the current. This is the result from the inductor voltage equation based on the waveform shown in Fig. 7. In addition it is possible to determine the current values for the phase A and B with the same approach or to use the symmetry in the waveforms to calculate them. The calculated value for the current waveforms according to Fig. 7 are

$$I_1 = \frac{V_1 \varphi}{6\omega L} \qquad (26)$$
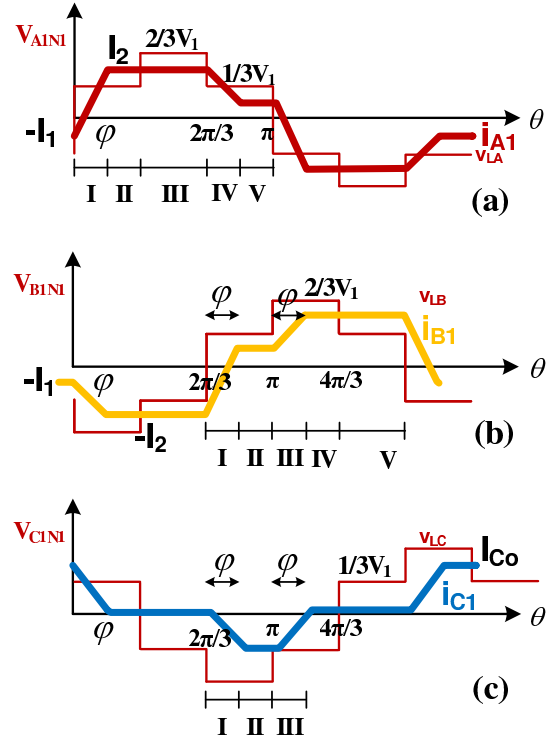
$$I_2 = \frac{V_1 \varphi}{2\omega L}. \qquad (27)$$

B. Power transfer calculation under the frozen leg at heavier loads

To calculate the transferred power in the case of a frozen leg, leg C in the secondary, the calculated inductor currents are used to calculate the transformer power in the primary side. The transformer phase voltages, V_{A1N1}, V_{B1N1}, and V_{C1N1}, are shown in Fig. 2. The next step is to multiply the inductor currents to these voltages in order to calculate the instantaneous power and perform an averaging in order to calculate the average power.

The power calculations are performed based on lossless model of the transformer. The inductor currents and transformer voltages are multiplied and averaged over a half cycle, for each phase. However, the analysis is based on the following assumptions: the input/output voltages are equal to the transformer turns ratio, there is no dead-time, the maximum value of the phase shift is 60°, and the components are ideal. Hence, a slight deviation from the measurement and theoretical values are expected. As it is explained earlier, these deviations are negligible and do not change the results and conclusion.

Fig. 8a shows the transformer current and voltage for phase A. A half cycle is divided into five intervals, where the power is calculated for each interval and then it is averaged over a half period to calculate the average power as

$$
\begin{aligned}
P_{AH} =& \frac{1}{\pi} \int_0^\pi V_{A1N1}(\theta) i_{A1}(\theta) d\theta = \\
& P_{AI} + P_{AII} + P_{AIII} + P_{AIV} + P_{AV}.
\end{aligned}
\qquad (28)
$$

For each interval, the power is calculated as

$$P_{AI} = \frac{1}{\pi}(\frac{1}{9}V_1 I_2 \ \varphi) \tag{29}$$

$$P_{AII} = \frac{1}{\pi}(\frac{1}{3}V_1 I_2 \ (\pi/3 - \varphi)) \tag{30}$$

$$P_{AIII} = \frac{1}{\pi}(\frac{2}{3}V_1 I_2 \ \pi/3) \tag{31}$$

$$P_{AIV} = \frac{1}{\pi}(\frac{2}{9}V_1 I_2 \ \varphi) \tag{32}$$

$$P_{AV} = \frac{1}{\pi}(\frac{1}{9}V_1 I_2 \ (\pi/3 - \varphi)). \tag{33}$$

The average power value of phase A can be calculated as

$$P_{AH} = \frac{10}{27}V_1 I_2 - \frac{1}{9}V_1 I_2 \ \varphi/\pi. \tag{34}$$

The same approach can be used to calculate the power for phase B and C. For phase B, the waveforms are shown in Fig. 8b. A half cycle is divided into five intervals and the average power is

$$P_{BH} = \frac{1}{\pi} \int_{2\pi/3}^{5\pi/3} V_{B1N1}(\theta) i_{B1}(\theta) d\theta = \\ P_{BI} + P_{BII} + P_{BIII} + P_{BIV} + P_{BV}. \tag{35}$$

For each interval, the power is calculated as

$$P_{BI} = \frac{1}{\pi}(-\frac{1}{9}V_1 I_2 \ \varphi) \tag{36}$$

$$P_{BII} = \frac{1}{\pi}(\frac{1}{9}V_1 I_2 \ (\pi/3 - \varphi)) \tag{37}$$

$$P_{BIII} = \frac{1}{\pi}(\frac{4}{9}V_1 I_2 \ \varphi) \tag{38}$$

$$P_{BIV} = \frac{1}{\pi}(\frac{2}{3}V_1 I_2 \ (\pi/3 - \varphi)) \tag{39}$$

$$P_{BV} = \frac{1}{\pi}(\frac{1}{9}V_1 I_2 \ \pi). \tag{40}$$

The average power value of the phase B can be calculated as

$$P_{BH} = \frac{10}{27}V_1 I_2 - \frac{2}{9}V_1 I_2 \ \varphi/\pi. \tag{41}$$

For phase C, as it is shown in Fig. 8c, three intervals are considered (the current is zero for some similar intervals in phase A and B). The average power over a half cycle is

$$P_{CH} = \frac{1}{\pi} \int_{2\pi/3}^{5\pi/3} V_{C1N1}(\theta) i_{C1}(\theta) d\theta = \\ P_{CI} + P_{CII} + P_{CIII}. \tag{42}$$

For each interval, the power is calculated as

$$P_{CI} = \frac{1}{\pi}(\frac{1}{2}I_{Co}\frac{2}{3}V_1 \ \varphi) \tag{43}$$

$$P_{CII} = \frac{1}{\pi}(I_{Co}\frac{2}{3}V_1 \ (\pi/3 - \varphi)) \tag{44}$$

$$P_{CIII} = \frac{1}{\pi}(\frac{1}{2}I_{Co}\frac{1}{3}V_1 \ \varphi). \tag{45}$$

The average power of phase C can be calculated as

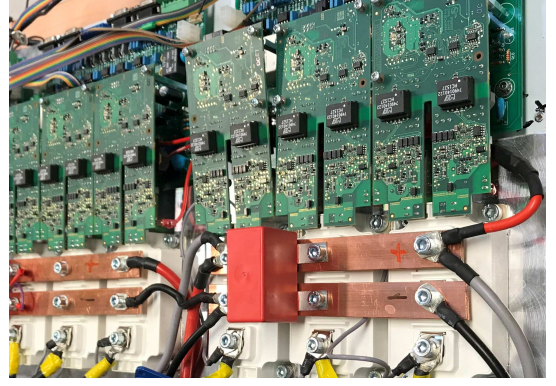$$P_{CH} = \frac{4}{27}V_1 I_2 - \frac{1}{9}V_1 I_2 \ \varphi/\pi. \tag{46}$$

Fig. 9. SiC power module and the driver used in the constructed converter.

Consequently, utilizing (34), (41) and (46), the total average power after leg C freeze at heavy loads, P_{tFH}, is

$$P_{tFH} = P_A + P_B + P_C = \frac{24}{27}V_1 I_2 - \frac{4}{9}V_1 I_2 \ \varphi/\pi \tag{47}$$

where by substitution of I_2 from (27) in this equation, the power can be written as

$$P_{tFH} = \frac{V_1^2}{2\omega L} \ \varphi \ (\frac{24}{27} - \frac{4\varphi}{9\pi}). \tag{48}$$

V. VERIFICATION

The constructed hardware, performed simulation and verification of the performed analysis and transition from light area to heavy load area in the context of a frozen leg operation mode are presented in this section.

A. Constructed hardware

In the context of a project a prototype with a power level of $50 \ kW$ is constructed. SiC power modules and nanocrystalline magnetics materials are utilized to achieve a higher power density and efficiency. The transformer leakage inductances are used as external energy storage components. To achieve similar leakage values, the primary and secondary windings are shifted in the core that is a toroidal core with Vitroperm 500 F materials [16].

For the semiconductor switches, SiC-based $300 \ A/1200 \ V$ modules are used (CAS300M12BM2) utilizing the dedicated drivers (PT62SCMD12). Each module includes a leg of the converter. Hence, in total 6 modules and drivers are used in the DC/DC converter. The command signals of the drivers are RS422 type and the interface circuits are constructed to change the signals to a TTL level. The driver has over-current protection and gate circuitry supply voltage protection. The driver has an independent processor to monitor and protect the module. It is a common case that the driver freezes the gate signal subject to a protective action. In this case, a physical reset signal is needed to restart the normal operation. Some sensor boards are designed and constructed to measure the dc bus voltages and the transformer currents. The control is performed through a C2000 Delfino microcontroller. Fig. 9 shows the power modules and dedicated drivers.
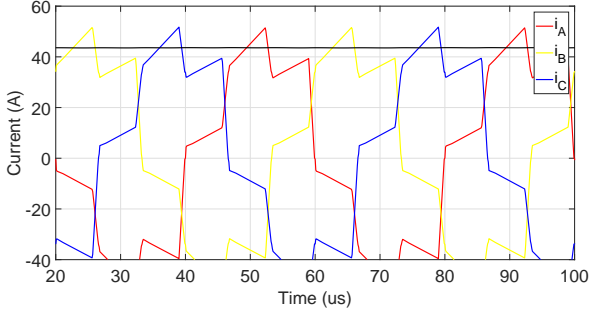
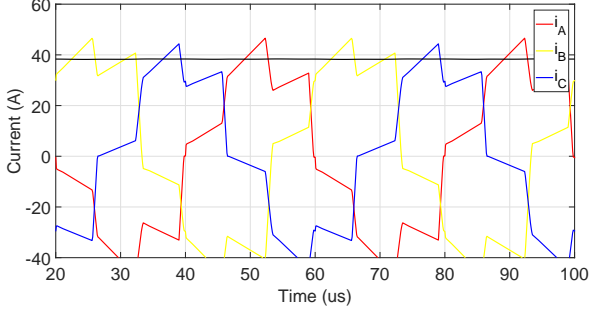Fig. 10. Simulation results for a normal operation condition at light loads.

Fig. 11. Simulation results after a frozen leg at light loads.

The value of the inductor is $16\ uH$ and the transformer turns ration is $n = 2$. The primary and secondary resistance of the transformer are $5\ mOhm$ and $2.5\ mOhm$, respectively.

B. Simulation parameters

The system is simulated in Matlab/Plecs. In order to achieve a better correlation with the experimental system, the dead-time, power Mosfet resistance, body diode voltage drop, and transformer losses are considered in the simulations. In addition, the dc bus inductances and resistances are modelled in the simulation as well.

The parameters of power Mosfets are considered constant in simulations. For the drain source resistance a value of $10\ mOhm$ is selected and for the body diode a voltage drop of $2\ V$ is chosen. The miller capacitance is ignored in simulation but a $2.2\ nF$ capacitance is selected for the drain source.

The switching frequency of the system is $25\ kHz$ which one cycle is $40\ us$. There is $1\ us$ dead time between the upper and lower switches in a leg.

C. Verification at light loads

To validate the performed analysis, simulations and experiments have been conducted where the results have shown an acceptable agreement between these parts, which are presented in this section. For an input voltage of $537\ V$, output voltage of $250\ V$ and a phase-shift angle of $\varphi = 10\ ^o$ transformer primary currents and the output dc currents are shown in Fig. 10 and Fig. 11 for a normal operation mode and a frozen leg condition, subsequently. Table I and Table II show the output currents for normal operation mode and frozen leg operation mode [14].

TABLE I
CONVERTER OUTPUT CURRENT IN A NORMAL OPERATING MODE AT A LIGHT LOAD.

Condition	Theory	Simulation	Measurement
$V_1 = 537\ V$ $V_2 = 250\ V$ $\varphi = 10^o$	$47.6\ A$	$43.6\ A$	$44.8\ A$

TABLE II
CONVERTER OUTPUT CURRENT IN A FROZEN LEG MODE AT A LIGHT LOAD.

Condition	Theory	Simulation	Measurement
$V_1 = 537\ V$ $V_2 = 250\ V$ $\varphi = 10^o$	$37.5\ A$	$38.3\ A$	$36.8\ A$

D. Verification at heavier loads

Fig. 12-15 show simulation and measurement results with an input voltage of $V_1 = 260\ V$. The operational conditions are stated in the figures caption. Results show that there is a good correlation between the theory, simulation and the measurement.

TABLE III
CONVERTER OUTPUT CURRENT IN A NORMAL OPERATING MODE AT A HEAVY LOAD.

Condition	Theory	Simulation	Measurement
$V_1 = 260\ V$ $V_2 = 130\ V$ $\varphi = 24^o$	$52\ A$	$50.8\ A$	$51\ A$

TABLE IV
CONVERTER OUTPUT CURRENT IN A FROZEN LEG MODE AT A HEAVY LOAD.

Condition	Theory	Simulation	Measurement
$V_1 = 260\ V$ $V_2 = 130\ V$ $\varphi = 24^o$	$35.95\ A$	$34\ A$	$35\ A$

Table III and Table IV show the output currents for normal operation mode and frozen leg operation mode. The values are presented for ideal calculations (without dead-time and losses), simulated values (including more realistic situation) and measurement results to provide a base for a quantitative comparison. The phase-shift value is $\varphi = 24^o$ and the dead-time is $1\ us$, which is equal to 4.5^o. If one switch is turned off $0.5\ us$ earlier than the case without dead time, it is equivalent $0.5\ us/40\ us$ which is $1/80$ of a full period that is $360/80 = 4.5^o$. Comparing simulations and measurements, there is a good match between the values. A maximum error of 5% can be seen under s frozen leg mode that can be the impact of the dead time.

E. Transition from light load to heavy load area in the context of a frozen leg operation

Two different behaviours are considered for a three-phase DAB under a frozen leg operation: light load behaviour and
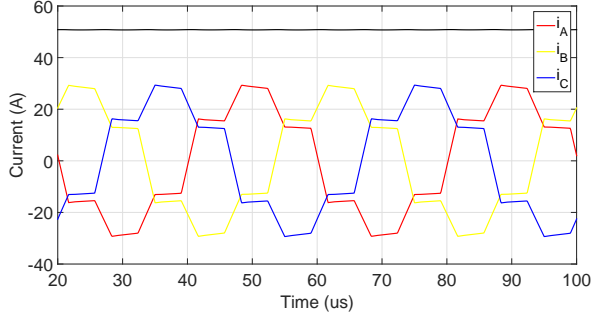
Fig. 12. Simulation of the converter operation in a healthy mode ($V_1 = 260\ V$, $V_2 = 130\ V$, $\varphi = 24^o$ and $I_o = 50.8\ A$).

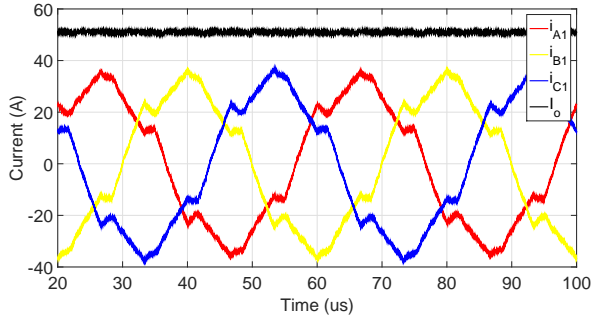Fig. 13. Measurement of the converter operation in a healthy mode ($V_1 = 260\ V$, $V_2 = 130\ V$, $\varphi = 24^o$ and $I_o = 51\ A$).
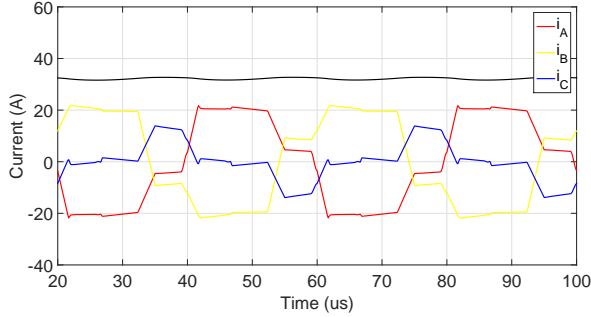

Fig. 14. Simulation of the converter operation in a frozen leg mode ($V_1 = 260\ V$, $V_2 = 130\ V$, $\varphi = 24^o$ and $I_o = 34\ A$).
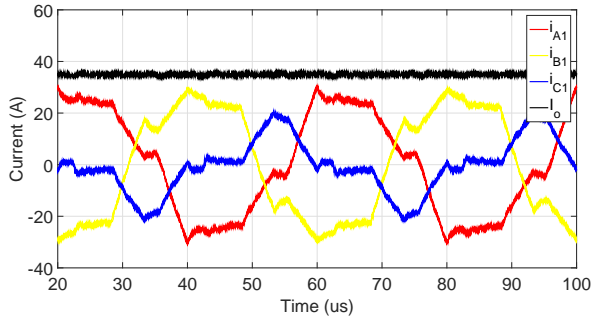

Fig. 15. Measurement of the converter operation in a frozen leg mode ($V_1 = 260\ V$, $V_2 = 130\ V$, $\varphi = 24^o$ and $I_o = 35\ A$).
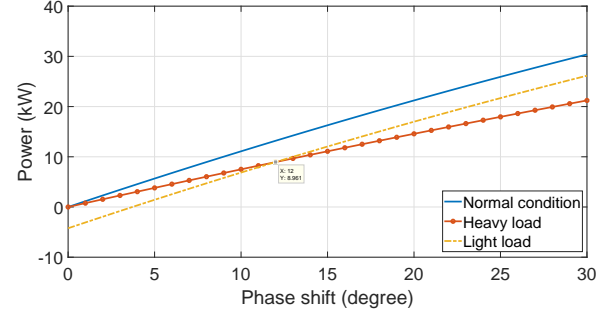

Fig. 16. Transferred power of a three-phase DAB converter in a normal operation mode, in a frozen leg mode at light loads and in a frozen leg mode at heavier loads.

heavy load behaviour. After a frozen leg mode, the power transfer equations are calculated for two modes based on (23) and (48). To calculate the boarder between light load and heavy load areas, the power equation can be solved to find out in which phase shift or power level the two equations intersect.

Fig. 16 shows the power transfer under a normal mode operation, a frozen leg converter mode at light loads and heavier loads as a function of phase shift. It is assumed that $alpha = 10^o$ and the operating parameters are: $f = 25\ kHz$, $L = 16\ uH$ and $V_1 = 500\ V$.

In this case, in a power level of $8.96\ kW$ or equivalently a phase-shift of 12° the mode is changed from light load to heavy load. This power level is a function of $alpha$ and input voltage under the condition that $V_1 = nV_2$. Any deviation from these conditions change the value of power for a mode change.

VI. CONCLUSIONS

For a three-phase DAB DC/DC converter a frozen leg fault mode is discussed in this paper. As a driver protection action, a leg can stop normal operation while the body diodes can continue to operate. It is demonstrated by analytical estimation, simulations and experiments that the converter can continue to operate after this fault mode but with a reduced power. Two different modes are analysed for a frozen leg operation where the boarder of mode transition is analytically determined. Simulations and measurement results show a strong correlation to the analytical formulation. The maximum error of the output current at frozen leg mode operation between theory, simulation and measurement is less than 5.5%.

ACKNOWLEDGMENT

REFERENCES

[1] R. W. De Doncker, D. M. Divan and M. H. Kheraluwala, "A three-phase soft-switched high-power-density DC-DC converter for high-power applications," in IEEE Transactions on Industry Applications, vol. 27, no. 1, pp. 63-73, Jan/Feb 1991.

[2] F. Krismer and J. W. Kolar, "Efficiency-Optimized High-Current Dual Active Bridge Converter for Automotive Applications," in IEEE Transactions on Industrial Electronics, vol. 59, no. 7, pp. 2745-2760, July 2012.

[3] B. Zhao, Q. Song, W. Liu and Y. Sun, "Overview of Dual-Active-Bridge Isolated Bidirectional DC/DC Connverter for High Fequency Link Power Conversion System," in IEEE Transactions on Power Electronics, vol. 29, no. 8, pp. 4091-4106, Aug. 2014.

[4] A. K. Tripathi, K. Hatua and S. Bhattacharya, "A comparative study of three-phase dual active bridge topologies and their suitability for D-Q mode control," 2012 IEEE Energy Conversion Congress and Exposition (ECCE), Raleigh, NC, 2012, pp. 1719-1724.

[5] N. H. Baars, J. Everts, H. Huisman, J. L. Duarte and E. A. Lomonova, "A 80-kW Isolated DC-DC Converter for Railway Applications," in IEEE Transactions on Power Electronics, vol. 30, no. 12, pp. 6639-6647, Dec. 2015.

[6] S. P. Engel, N. Soltau, H. Stagge and R. W. De Doncker, "Dynamic and Balanced Control of Three-Phase High-Power Dual-Active Bridge DC-DC Converters in DC-Grid Applications," in IEEE Transactions on Power Electronics, vol. 28, no. 4, pp. 1880-1889, April 2013.

[7] H. S. H. Wang, F. Blaabjerg and M. Pecht, Reliability of Power Electronic Converter Systems, IET, 2015, ISBN: 978-1-84919-901-8.

[8] S. Haghbin, "Electrical failure mode and effect analysis of a 3.3 kW on-board vehicle battery charger," presented in 18th European Conference on Power Electronics and Applications (EPE'16 ECCE Europe), Karlsruhe, 2016, pp. 1-10.

[9] Z. Qin, Y. Shen, P. C. Loh, H. Wang and F. Blaabjerg, "A Dual Active Bridge Converter With an Extended High-Efficiency Range by DC Blocking Capacitor Voltage Control," in IEEE Transactions on Power Electronics, vol. 33, no. 7, pp. 5949-5966, July 2018.

[10] Y. Song and B. Wang, "Survey on Reliability of Power Electronic Systems," in IEEE Transactions on Power Electronics, vol. 28, no. 1, pp. 591-604, Jan. 2013.

[11] W. Zhang, D. Xu, P. N. Enjeti, H. Li, J. T. Hawke and H. S. Krishnamoorthy, "Survey on Fault-Tolerant Techniques for Power Electronic Converters," in IEEE Transactions on Power Electronics, vol. 29, no. 12, pp. 6319-6331, Dec. 2014.

[12] R. Bono, R. Alexander, A. Dorman, Yong-Jin Kim and J. Reisdorf, "Analyzing reliability - a simple yet rigorous approach," in IEEE Transactions on Industry Applications, vol. 40, no. 4, pp. 950-957, July-Aug. 2004.

[13] U. M. Choi, F. Blaabjerg and S. Jrgensen, "Power Cycling Test Methods for Reliability Assessment of Power Device Modules in Respect to Temperature Stress," in IEEE Transactions on Power Electronics, vol. 33, no. 3, pp. 2531-2551, March 2018.

[14] S. Haghbin, F. Blaabjerg, F. Yazdani and A. S. Bahman, "Frozen leg operation of a three-phase dual active bridge DC/DC converter at light loads," presented in IEEE Applied Power Electronics Conference and Exposition (APEC), San Antonio, TX, USA, 2018, pp. 3385-3391.

[15] S. P. Engel, N. Soltau, H. Stagge and R. W. De Doncker, "Dynamic and Balanced Control of Three-Phase High-Power Dual-Active Bridge DC-DC Converters in DC-Grid Applications," in IEEE Transactions on Power Electronics, vol. 28, no. 4, pp. 1880-1889, April 2013.

[16] S. Haghbin, M. Alatalo, F. Yazdani, T. Thiringer and R. Karlsson, "The Design and Construction of Transformers for a 50 kW Three-Phase Dual Active Bridge DC/DC Converter," 2017 IEEE Vehicle Power and Propulsion Conference (VPPC), Belfort, 2017, pp. 1-5.